American Mineralogist, Volume 87, pages 227–237, 2002

Sulfur saturation limits in silicate melts and their implications for core formation scenarios for terrestrial planets

ASTRID HOLZHEID* AND TIMOTHY L. GROVE

Department of Earth, Atmospheric and Planetary Sciences, Massachusetts Institute of Technology, Cambridge, Massachusetts 02139-4307, U.S.A.

ABSTRACT

This study explores the controls of temperature, pressure, and silicate melt composition on S solubility in silicate liquids. The solubility of S in FeO-containing silicate melts in equilibrium with metal sulfide increases significantly with increasing temperature but decreases with increasing pressure. The silicate melt structure also exercises a control on S solubility. Increasing the degree of polymerization of the silicate melt structure lowers the S solubility in the silicate liquid. The new set of experimental data is used to expand the model of Mavrogenes and O'Neill (1999) for S solubility in silicate liquids by incorporating the influence of the silicate melt structure. The expected S solubility in the ascending magma is calculated using the expanded model. Because the negative pressure dependence of S solubility is more influential than the positive temperature dependence, decompression and adiabatic ascent of a formerly S-saturated silicate magma will lead to S undersaturation. A primitive magma that is S-saturated in its source region will, therefore, become S-undersaturated as it ascends to shallower depth. In order to precipitate magmatic sulfides, the magma must first cool and undergo fractional crystallization to reach S saturation. The S content in a metallic liquid that is in equilibrium with a magma ocean that contains ~200 ppm S (i.e., Earth's bulk mantle S content) ranges from 5.5 to 12 wt% S. This range of S values encompasses the amount of S (9 to 12 wt%) that would be present in the outer core if S is the light element. Thus, the Earth's proto-mantle could be in equilibrium (in terms of the preserved S abundance) with a core-forming metallic phase.

INTRODUCTION

The solubility behavior of S in silicate liquids that coexist with metal-sulfide phases is of crucial importance for modeling the genesis of sulfide ores that are associated with mafic and ultramafic igneous rocks. Magmatic sulfides are generally considered to have formed from S-oversaturated silicate magmas. If the S solubility limit of a silicate melt increases as pressure decreases and temperature drops, a sulfide ore would not separate by a simple saturation and settling-out process, because the magma will never achieve sulfide saturation. Furthermore, knowledge of the S solubility limits in silicate melts will improve our understanding of early differentiation processes in the Earth and other planetary bodies. The S abundance in the silicate mantle after cessation of the formation of the planet's core can potentially provide information about the nature of the core-forming process. Models of the sulfide saturation limits can be applied to abundances in mantle rocks to infer possible conditions of core-mantle separation processes.

Sulfur solubility in silicate melt has been shown to be dependent upon temperature, pressure, oxygen fugacity, sulfur fugacity, and melt composition. In a pioneering study, Fincham and Richardson (1954) studied the behavior of S in binary and ternary silicate and aluminate melts under controlled temperature, oxygen fugacity, and sulfur fugacity conditions at ambient pressure. Following this pioneering work, Abraham et al. (1960) and Abraham and Richardson (1960) reported results of the dependence of dissolved S in binary and ternary silicate and aluminate slags on oxygen fugacity and sulfur fugacity at ambient pressure. Haughton et al. (1974) examined multi-component silicate liquids and the influence of temperature, oxygen fugacity, and sulfur fugacity on S solubility in silicate melts at ambient pressure. Wallace and Carmichael (1992) subsequently expanded this model to low-pressure conditions. Poulson and Ohmoto (1990) compiled experimental studies, mainly from the materials science literature, that investigated the S solubility limits (SSL) in silicate and oxide melts and provided a number of parameterizations of the dependences of SSL on temperature (T), pressure (P), oxygen fugacity (f_{O_2}), sulfur fugacity (f_{S_2}), and chemical composition (X) of the coexisting phases. They also explored SSL-variations under hydrous conditions. Poulson and Ohmoto (1990) found complex correlations among T, P, f_{O_2}, f_{S_2}, and X that prohibited construction of a general equation to predict SSL. Poulson and Ohmoto (1990) used the available experimental data to define three distinct groups, and they proposed that the speciation of S took place differently in each group. FeO-content was found to be the most sensitive compositional parameter. The experimentally derived correlations of the SSL with the FeO-content were found to be in reasonable agreement with trends observed in natural melts and in sulfide-saturated natural glasses (see

* Current address: Westfälische Wilhelms-Universität Münster, Institut für Mineralogie, Corrensstrasse 24, 48149 Münster, Germany. E-mail: holzheid@uni-muenster.de

Poulson and Ohmoto 1990 for references). However, the experimentally derived relationships between the SSL and temperature and, especially, pressure were less well defined. Wendlandt (1982) found that the SSL decreased with increasing pressure and increased with increasing temperature. In contrast, Mysen and Popp (1980) found increasing S concentration levels in silicate melts with increasing pressure and temperature. The most recent study by Mavrogenes and O'Neill (1999) is in agreement with the findings of Wendlandt (1982) on the pressure and temperature dependence of S solubility in silicate liquid.

The aim of this study is to explore the influence of temperature, pressure, silicate melt composition, and sulfide melt composition on S saturation and to attempt to reconcile discrepancies among the previous experimental studies. We use the experimental data on SSL to derive a single expression that describes the SSL in silicate liquids as function of temperature, pressure, and silicate melt composition. We also use the experimental data on SSL and the observed/inferred S abundances in planetary bodies to discuss possible metal sulfide-silicate segregation processes.

EXPERIMENTS

Experimental techniques

Sulfur saturation experiments were carried out in 1/2" solid-medium piston-cylinder apparatuses (Boyd and England 1960) over a temperature range of 1300 to 1600 °C and a pressure range from 0.9 to 2.7 GPa. Starting materials consisted of powdered mixtures of iron sulfide (Fe = 60 at%, S = 40 at%), elemental sulfur, and oxide mixes and/or silicate glasses. Andesite, basalt, and ultramafic silicate starting materials were chosen to explore the controls of silicate melt composition, especially the major element oxide contribution, on the S solubility in the silicate liquid. The compositions of the silicate starting materials are listed in Table 1. In some of the experiments, the starting mixtures were initially enriched in olivine by adding an oxide mix with the composition of forsterite. Mixing proportions were approximately 50% metal sulfide + sulfur and 50% synthetic silicate + forsterite by weight. Starting materials (on average 20 mg) were packed into olivine capsules fabricated from single crystal San Carlos olivine (Fo_{89-91}, OD = 4.3 mm, ID = 2.2 mm, capsule length = 3.9 mm, "sample" length = 1.7 mm) to avoid contamination of the sample with capsule material (e.g., graphite enrichment of the experimental charge by using graphite capsules). The olivine crucibles were enclosed in sleeves of solid Al_2O_3 ceramic and were then centered using MgO spacers in the hot zone of the graphite heater. The graphite furnace was contained in a sleeve of pressed $BaCO_3$ pressure medium. In the first set of experiments, the olivine crucible was inserted into a 1/4"-diameter MgO sleeve. The graphite heater failed in most of these experiments within the first 10 hours, due to severe plastic deformation of the olivine crucible, the MgO sleeve, and finally the graphite heater. The problem of the failure of the graphite heater was overcome by the use of the sleeves of solid Al_2O_3 ceramic surrounding the olivine crucibles. The sample pressure was corrected for friction associated with the assemblies of all experiments. The temperature of the charge was measured and controlled using a W_3Re_{97}–$W_{25}Re_{75}$ thermocouple. Experimental run durations were 10 minutes to 25 hours. All piston-cylinder assemblies were pressurized cold to about 0.7 GPa, heated to 865 °C at 100 °C/min, and pressurized to the final pressure while the temperature was kept constant at 865 °C for 6 minutes. The temperature was then raised to the experiment temperature at a rate of 50 °C/min while the final pressure was kept constant on the sample. Microcracking of the olivine capsule during pressurization resulted in infiltration of some starting material into the wall of the olivine capsule. Nevertheless, liquid metal sulfide, silicate melt, Ca-pyroxene, and/or olivine crystals coexisted within the capsule in all experimental charges. The charges were quenched by turning off the power. The sample temperature dropped below 500 °C within the first 10 seconds after turning off the power to the graphite heater and the sample pressure was released instantaneously. The charges were mounted in epoxy, cut longitudinally through the center of the olivine capsule, and polished for electron microprobe analysis. The samples ranged in size from 1.5 to 2 mm in width and from 1.3 to 0.5 mm in length depending on experiment conditions. Experimental conditions are given in Table 2.

TABLE 1. Silicate starting compositions

Wt%	SSKOM	BK	AD	85–41c	I-10–08	SB
SiO_2	50.1	49.1	50.9	57.8	50.2	50.0
TiO_2	0.33			0.60	2.30	
Al_2O_3	10.6	14.1	13.8	14.5	10.2	15.3
Cr_2O_3	0.41				0.06	
FeO	11.0	7.00		5.74	4.49	8.61
MnO	0.36			0.11	0.09	
MgO	17.2	10.6	10.4	9.14	7.48	12.4
CaO	9.49	19.2	24.9	8.17	6.12	11.6
Na_2O	0.37			3.11	1.29	2.04
K_2O	0.07			0.71	10.5	
NiO	0.09					
P_2O_5				0.15	1.81	
H_2O				1.64	2.34	

Notes: SSKOM = synthetic komatiite added as oxide mixture to the starting mixture, composition B of Kinzler and Grove (1985); BK = synthetic MgO-rich basalt added as powdered silicate glass, composition of Holzheid and Palme (1996); AD = synthetic anorthite-diopside eutectic silicate added as powdered silicate glass, composition of Holzheid and Palme (1996); 85–41c = basaltic natural volcanic sample, composition given in Baker et al. (1994); I-10–08 = wyomingite from the Leucite Hills. A representative composition from Carmichael (1967) is presented; SB = synthetic basalt added as oxide mixture, basaltic silicate starting composition of Holzheid et al. (2000).

Analytical techniques

Back-scattered electron (BSE) imaging and energy-dispersive spectrometry (EDS) analyzes were used to distinguish between the coexisting phases in the experimental charges. The phases present in each charge are given in Table 2. Quantitative analyzes were obtained by wavelength-dispersive spectrometry (WDS) using a JEOL 733 Superprobe electron microprobe with 15 keV accelerating voltage and a beam current of 10 nA. Spot size ranged from 1 to 30 μm depending on the analyzed phases. The data were reduced with the CITZAF program (Armstrong 1995). Counting times were 40 s for major elements (Mg, Si, Fe) in the silicate phases, and for all components in the metal sulfide phases. Longer counting times (up to 600 s counting on peak) were used for the trace-element

TABLE 2. Experimental parameters

	No.	T (°C)	P (GPa)	Time (h)	ΔIW	Starting mixture	Phases present	
FeS-SSKOM 13	C 201	1450	1.0	0.2	–1.8	SSKOM+FeS+S	gl,ms	(q)
FeS-SSKOM 12	C 200	1450	1.0	0.8	–1.4	SSKOM+FeS+S	gl,ms	q
FeS-SSKOM 11	C 199	1450	1.0	1.5	–1.4	SSKOM+FeS+S	gl,ol,ms	q
FeS-SSKOM 7*	C 168	1450	1.0	3.0	–1.6	SSKOM+FeS+S	gl,px,ol,ms	
FeS-SSKOM 5*	C 166	1450	1.0	6.2	–1.7	SSKOM+FeS+S	gl,px,ol,ms	
FeS-SSKOM 6*	C 167	1450	1.0	12	–1.6	SSKOM+FeS+S	gl,px,ol,ms	†
FeS-SSKOM 1*	B 542	1425	1.5	20	–1.4	SSKOM+FeS	gl,px,ol,ms	(q)†
FeS-SSKOM 2*	B 544	1450	1.6	20	–1.4	SSKOM+FeS	gl,px,ol,ms	(q)†
FeS-SSKOM 14	C 202	1500	0.9	7.3	–1.0	SSKOM+FeS+S	gl,ol,ms	q
FeS-SSKOM 25	B 715	1500	1.0	5.5	–1.4	SSKOM+FeS+S	gl,ol,ms	
FeS-SSKOM 26	B 716	1500	1.0	5.5	–1.5	SSKOM+FeS+S	gl,ol,ms	
FeS-SSKOM 15	C 203	1500	1.4	5.1	–1.3	SSKOM+FeS+S	gl,ol,ms	q
FeS-SSKOM 16	C 204	1500	2.0	4.8	–1.3	SSKOM+FeS+S	gl,ol,ms	(q)
FeS-SSKOM 27 R	B 718	1500	2.0	6.0	–1.5	SSKOM+FeS+S	gl,ol,ms	
FeS-SSKOM 23	B 654	1500	2.4	12	–2.1	SSKOM+FeS+S	pm,ms	
FeS-SSKOM 17	C 205	1500	2.5	5.0	–1.7	SSKOM+FeS+S	pm,ms	
FeS-SSKOM 24	B 660	1500	2.7	11	–2.0	SSKOM+FeS+S	pm,ms	
FeS-BK 2*	B 560	1300	1.0	25		BK+FeS+S	sl,ms	
FeS-BK 10	B 590	1300	1.0	16		BK+FeS+S+Fo	sl,ms	
FeS-BK 11	B 594	1350	1.0	17	–1.3	BK+FeS+S+Fo	pm,ms	
FeS-BK 12	B 607	1400	1.0	15	–1.3	BK+FeS+S+Fo	pm,ms	
FeS-BK 9	B 589	1450	1.0	12	–1.6	BK+FeS+S+Fo	gl,ol,ms	(q)†
FeS-BK 8	B 587	1525	1.0	10	–1.6	BK+FeS+S+Fo	gl,ol,ms	q
FeS-BK 4*	B 562	1600	1.0	9.0	–1.4	BK+FeS+S+Fo	gl,ol,ms	q
FeS-BK 13	B 717	1600	1.0	5.5	–1.3	BK+FeS+S+Fo	gl,ol,ms	q
FeS-AD 1	B 586	1450	1.0	12	–1.8	AD+FeS+S+Fo	gl,ol,ms	(q)†
FeS-85-41c-1	B 609	1450	1.0	12	–1.7	85-41c+FeS+S	gl,ol,ms	
FeS-I-10-08-1	B 610	1450	1.0	12	–1.7	I-10-08+FeS+S	gl,ol,ms	†
FSOs-15-6	B 503	1370	1.4	4.0	–2.0	SB+FeS+SC	gl,px,ol,ms	
FSOs-15-7	C 143	1370	1.4	23	–1.9	SB+FeS+SC	gl,px,ol,ms	

Notes: SSKOM = synthetic komatiite, see Table 1; BK = MgO-rich basalt, see Table 1; AD = anorthite-diopside eutectic silicate, see Table 1; 85–41c = basaltic natural volcanic sample, see Table 1; I-10–08 = wyomingite from the Leucite Hills, see Table 1; SB = synthetic basalt, see Table 1; FeS = metal sulfide $Fe_{1.45}S$; S = elemental sulfur; Fo = oxide mix of forsterite composition; SC = single San Carlos olivine crystals (37 to 53 μm in size); gl = silicate glass; ms = metal sulfide; px = pyroxene; ol = olivine; pm,ms = partly molten silicate starting material, metal sulfide phase in silicate melt pockets; sl,ms = metal sulfide phase in subliquidus silicate starting material; q,(q) = width of quenched silicate rim > 50 μm (<50 μm); R = reversal, increase of pressure to 2 GPa after charge was at 1500 °C and 1 GPa for 5.6 h.

* Olivine capsule in MgO sleeve, otherwise olivine capsule in alumina sleeve.

† Plotted in Figure 2 (P-dependence on SSL) as experiments at 1425 and 1450 °C; ΔIW = calculated oxygen fugacity prevailed in the experiments relative to the Iron-Wüstite (IW) buffer (see text for detail).

analyzes of S in the silicate phases.

The liquid metal sulfide quenched into two immiscible liquids that consisted of a mixture of an Fe-rich, S-poor phase and an Fe-sulfide phase close to stoichiometric MS, where M is Fe and minor amounts of other metallic elements that were concentrated in the metal sulfide liquid (i.e., Ni or Co). Average element concentrations in the metal phases were determined by measuring the modal abundances of S-poor and S-rich phases using BSE-image analysis software and recombining the two phases in the appropriate proportions. Quantitative analyzes of metal phases that were smaller than 50 μm were obtained using a larger electron beam spot size (up to 30 μm). Chemical compositions of the coexisting phases in the experimental charges are given in Tables 3–5.

EXPERIMENTAL RESULTS

Concentrations of S in the silicate melt range from 750 to about 3300 ppm over the investigated temperature and pressure conditions (1350–1600 °C, 0.9–2.7 GPa). The S content in the silicate liquid remained constant after about 3 hours as shown by "time-series" experiments indicating an approach to steady state (Table 2; experiments FeS-SSKOM 5–7,11–13). The apparent higher S concentrations in the silicate melt in experiments with shorter experiment durations might be related to finely disseminated metal sulfide droplets in the silicate liquid that were not agglomerated into larger metal sulfide melt blebs. In the experimental charges with experiment durations of ≥ 3 hours, large sulfide melt blebs were always present.

Attainment of equilibrium was also demonstrated by a reversal experiment (labeled "R" in Table 2). In this experiment, the experimental charge was held at constant temperature (1500 °C) and pressure P_1 (1 GPa) for a few hours (5.6 h). The sample pressure was then increased to pressure P_2 (2 GPa; $P_2 > P_1$) while the temperature remained constant. The charge was held at constant temperature and pressure P_2 for 6 hours. The experiment was quenched by turning off the power. As the S solubility in silicate liquid decreases with increasing pressure (see below) the S content in the starting silicate liquid (P_1) was higher than the equilibrium S content in the silicate liquid at P_2 after increasing the pressure. Thus S migrated from silicate melt to the metal sulfide, i.e., the S content in the silicate liquid decreased. The agreement between the S content in the silicate melt of experiments initially brought up to P_2 and the reversed experiment ($P_1 \rightarrow P_2$) confirms that equilibrium has been achieved. Reproducibility of experimental results was tested by repeating experiments at identical T-P experiment conditions (e.g., experiments FeS-SSKOM 25 and FeS-SSKOM 26;

TABLE 3. Silicate melt compositions in wt%

		SiO_2	TiO_2	Al_2O_3	Cr_2O_3	FeO	MnO	MgO	CaO	Na_2O
FeS-SSKOM 13	*5*	53.0 (4)	0.338 (14)	10.8 (4)	0.243 (10)	7.78 (23)	0.220 (6)	17.9 (12)	10.1 (4)	0.039 (9)
FeS-SSKOM 12	*10*	50.4 (2)	0.271 (6)	8.36 (12)	0.277 (4)	12.3 (1)	0.254 (6)	19.8 (5)	7.97 (17)	0.003 (2)
FeS-SSKOM 11	*10*	50.8 (2)	0.274 (10)	8.77 (16)	0.192 (3)	12.8 (2)	0.245 (6)	17.9 (7)	8.51 (20)	0.057 (9)
FeS-SSKOM 7	*12*	50.3 (1)	0.357 (4)	11.1 (1)	0.107 (3)	9.86 (3)	0.218 (3)	16.8 (1)	10.4 (1)	0.269 (8)
FeS-SSKOM 5	*17*	49.7 (1)	0.397 (5)	12.1 (1)	0.091 (2)	8.76 (6)	0.222 (4)	16.5 (1)	11.8 (1)	0.292 (11)
FeS-SSKOM 6	*16*	50.8 (1)	0.329 (3)	10.5 (1)	0.118 (2)	9.23 (5)	0.203 (4)	18.4 (1)	10.2 (1)	0.229 (10)
FeS-SSKOM 1	*8*	46.0 (2)	1.01 (2)	16.2 (3)	0.122 (7)	13.5 (2)	0.336 (11)	8.52 (75)	13.1 (3)	0.659 (68)
FeS-SSKOM 2	*10*	46.0 (4)	0.624 (35)	14.9 (4)	0.128 (8)	13.5 (5)	0.329 (3)	11.5 (7)	12.0 (2)	0.032 (31)
FeS-SSKOM 14	*5*	51.0 (4)	0.367 (12)	10.1 (4)	0.104 (10)	17.2 (7)	0.290 (11)	10.5 (5)	8.99 (45)	0.156 (19)
FeS-SSKOM 25	*20*	50.0 (1)	0.247 (4)	8.55 (12)	0.149 (4)	12.8 (1)	0.252 (3)	20.7 (3)	7.09 (9)	0.186 (7)
FeS-SSKOM 26	*35*	50.6 (1)	0.280 (2)	9.30 (5)	0.149 (4)	10.6 (0)	0.233 (2)	19.9 (2)	8.09 (4)	0.205 (8)
FeS-SSKOM 15	*5*	49.2 (7)	0.286 (29)	9.77 (85)	0.153 (11)	14.0 (3)	0.255 (15)	17.8 (26)	8.16 (76)	0.088 (12)
FeS-SSKOM 16	*10*	47.0 (2)	0.557 (7)	14.2 (2)	0.118 (4)	12.5 (2)	0.252 (4)	9.65 (48)	13.9 (2)	0.306 (14)
FeS-SSKOM 27 R	*8*	47.1 (1)	0.497 (11)	14.5 (3)	0.125 (2)	9.87 (18)	0.232 (3)	12.6 (9)	13.3 (3)	0.241 (44)
FeS-SSKOM 23	*5*	50.0 (5)	0.209 (10)	9.66 (65)	0.265 (11)	5.92 (11)	0.264 (8)	22.6 (3)	10.8 (4)	0.236 (15)
FeS-SSKOM 17	*6*	50.8 (3)	0.126 (24)	6.95 (33)	0.279 (19)	8.93 (24)	0.247 (6)	22.2 (6)	10.0 (6)	0.049 (9)
FeS-SSKOM 24	*10*	47.7 (11)	0.211 (19)	14.6 (17)	0.416 (40)	6.11 (22)	0.306 (19)	22.4 (6)	8.47 (79)	0.135 (24)
FeS-BK 11	*15*	44.7 (2)	n.d.	16.2 (3)	n.d.	11.9 (1)	n.d.	8.08 (27)	16.8 (2)	n.d.
FeS-BK 12	*10*	44.8 (6)	n.d.	17.8 (2)	n.d.	11.9 (1)	n.d.	6.25 (39)	17.6 (4)	n.d.
FeS-BK 9	*13*	47.0 (1)	n.d.	10.6 (1)	n.d.	8.63 (3)	n.d.	16.4 (2)	16.7 (1)	n.d.
FeS-BK 8	*19*	46.4 (1)	n.d.	10.1 (1)	n.d.	9.27 (5)	n.d.	19.7 (4)	14.0 (2)	n.d.
FeS-BK 4	*9*	47.8 (2)	n.d.	11.1 (4)	n.d.	11.2 (2)	n.d.	11.8 (8)	17.1 (3)	n.d.
FeS-BK 13	*5*	42.2 (3)	n.d.	13.4 (6)	n.d.	12.6 (1)	n.d.	22.1 (15)	8.72 (49)	n.d.
FeS-AD 1	*14*	46.3 (1)	n.d.	12.0 (1)	n.d.	7.06 (3)	n.d.	17.2 (5)	16.5 (2)	n.d.
FeS-85-41c-1	*15*	51.7 (2)	0.562 (5)	13.5 (1)	0.015 (6)	7.93 (2)	0.149 (5)	13.8 (1)	8.15 (9)	3.17 (8)
FeS-I-10-08-1	*15*	50.8 (1)	2.12 (1)	7.79 (4)	0.051 (6)	8.37 (4)	0.113 (4)	14.5 (1)	4.16 (3)	0.729 (13)
FSOs-15-6	*10*	50.1 (8)	1.07 (50)	19.9 (4)	0.078 (35)	7.02 (31)	0.107 (16)	5.22 (14)	7.48 (22)	6.38 (15)
FSOs-15-7	*10*	50.5 (2)	0.081 (3)	20.2 (2)	0.013 (3)	7.89 (9)	0.130 (4)	6.90 (29)	10.1 (1)	4.46 (5)

Notes: Numbers in italic font are numbers of individual analyzes. Numbers in parentheses are 1 σ standard deviations of the mean. The entry should be read 53.0 ± 0.4 wt%. Experiments FeS-BK 1 and FeS-BK 10 are not included as the metal sulfide phase coexisted with subliquidus silicate starting material. n.d. = not determined. <d.l. = below detection limit. *nbo/t* = ratio of non-bridging O atoms to tetrahedrally coordinated cations in the silicate (calculated after Mysen 1988).

experiments FeS-BK 4 and FeS-BK 13).

The experiments carried out at $T \geq 1400$ °C, $P = 1$ GPa and at $T = 1500$ °C, $P < 2.4$ GPa contained silicate melt as the dominant phase, along with olivine (ol), and/or pyroxene (px) crystals and a coexisting sulfide phase. The silicate melt quenched to a homogeneous glass in the center of the charges. In some of the experiments, quench growth is present as a thin layer around px and ol crystals and along the inner wall of the olivine capsule (see Table 2). The crystalline phases varied in size within the charges with crystals as large as 500 × 200 μm to more typical crystal sizes of 100 × 100 μm. The silicate glass regions also varied in size from tiny patches between crystalline phases and quench growth-free regions as large as 800 × 400 μm. The S content of the coexisting crystalline phases (px and ol) is below the detection limit (d.l. = 80 ppm).

In the lower temperature experiments ($T < 1425$ °C) conducted at higher pressures ($P > 2.4$ GPa), silicate melt was trapped in small silicate melt pockets together with metal sulfide blebs. In these dominantly crystalline experiments, it was still possible to determine the SSL.

The dependence of S solubility on temperature at isobaric conditions (1 GPa) is illustrated in Figure 1. The S content in the silicate melt increases with increasing temperature.

The dependence of S solubility on pressure at isothermal conditions is illustrated in Figure 2. The S content in the silicate melt decreases with increasing pressure. The pressure dependence is more pronounced at lower pressures than at higher pressures.

The dependence of S solubility on the silicate liquid composition at isothermal (1450 °C) and isobaric (1 GPa) conditions is illustrated in Figure 3. The dependence is plotted as the concentration of S vs. the *nbo*/*t*-value of the silicate liquid, i.e., the ratio of non-bridging oxygen anions to tetrahedrally coordinated cations in the silicate that is a measure of the degree of polymerization of the silicate melt structure (Mysen 1988). Due to the limited number of experiments on more polymerized silicate liquids, the S solubility dependence on silicate liquids with lower *nbo*/*t*-ratios is not well defined. However, the S content in relatively polymerized silicate liquids is consistent with the values obtained by other workers. The S solubility in silicate liquid shows an increase with higher *nbo*/*t*-values. More S dis-

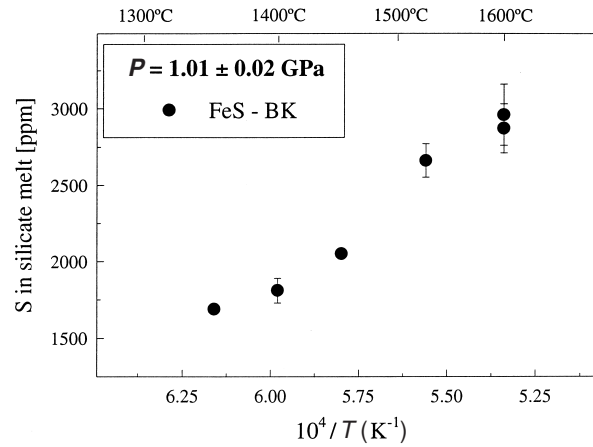

FIGURE 1. Sulfur concentration in the silicate melt as a function of temperature at constant pressure (1 GPa).

TABLE 3—*Extended*

K_2O	NiO	S	Total	*nbo/t*
0.043 (3)	0.031 (6)	0.173 (6)	100.7	1.16
0.031 (2)	0.031 (4)	0.230 (3)	99.9	1.46
0.033 (2)	0.015 (3)	0.223 (6)	99.8	1.38
0.051 (3)	<d.l.	0.199 (2)	99.7	1.23
0.052 (3)	<d.l.	0.191 (2)	100.1	1.20
0.045 (3)	<d.l.	0.203 (2)	100.3	1.29
0.298 (57)	0.035 (7)	0.178 (26)	100.0	0.91
0.168 (46)	0.009 (3)	0.185 (10)	99.4	1.05
0.035 (2)	0.028 (7)	0.332 (10)	99.1	1.11
0.041 (1)	0.019 (3)	0.291 (8)	100.3	1.51
0.047 (1)	0.013 (2)	0.327 (1)	99.7	1.40
0.036 (4)	0.018 (6)	0.239 (8)	100.0	1.39
0.100 (6)	0.020 (5)	0.215 (7)	98.8	1.02
0.075 (11)	<d.l.	0.194 (8)	98.7	1.05
0.004 (1)	0.028 (3)	0.161 (14)	100.1	1.47
<d.l.	0.008 (3)	0.206 (30)	99.8	1.62
<d.l.	<d.l.	0.174 (29)	100.5	1.22
n.d.	0.033 (5)	0.169 (3)	97.9	0.98
n.d.	0.018 (7)	0.181 (8)	98.5	0.86
n.d.	<d.l.	0.205 (2)	99.5	1.48
n.d.	0.015 (5)	0.266 (11)	99.8	1.62
n.d.	0.031 (6)	0.296 (20)	99.3	1.31
n.d.	0.011 (3)	0.287 (16)	99.3	1.59
n.d.	<d.l.	0.217 (3)	99.3	1.42
0.765 (12)	<d.l.	0.150 (3)	99.9	0.95
8.39 (8)	<d.l.	0.213 (4)	97.2	1.15
0.839 (23)	<d.l.	0.075 (13)	98.3	0.46
0.159 (3)	<d.l.	0.126 (32)	100.6	0.56

solves in depolymerized than in polymerized silicate liquids, suggesting that S reacts preferentially with the non-bridging oxygen atoms in the melt. The S solubility seems to achieve a constant level at *nbo/t*-values of ~0.9 to 1.6 by excluding FeS-85-41c, whereas the S content in the silicate melt increases by a factor of 1.4 within an *nbo/t*-range of about 0.5 to 0.9. However, once the *nbo/t*-value is above 1, the melt composition has less influence on the S solubility in silicate liquid.

Also plotted in Figure 3 are recalculated S concentrations in basaltic silicate liquids of FeS-BK experiments of this study (gray downward triangles) and experiments reported by Holzheid et al. 2000 (gray cross-haired triangles). Basaltic silicate liquid coexisted with crystalline olivine and metal sulfide melt in the latter experiments. The data are included in the Tables. Experimental conditions were 1370 °C and 1.4 GPa. The S concentrations are recalculated to 1450 °C and 1 GPa using the combined *T-P* dependence determined in this study (see below, Equation 2 with fit parameters of Table 7a). Uncertainties in the recalculated S concentrations are within factors of about 1.4 (FSOs-15–7) and 1.2 (FSOs-15–6). Both experiments further affirm a significant dependence of the S solubility on the *nbo/t*-ratio in polymerized rather than in depolymerized silicate liquids.

Because experimental set-ups in all of our experiments were identical and the mole fraction ratio $FeO^{\text{silicate liquid}}/Fe^{\text{metal sulfide}}$ is approximately constant in all experiments, a significant systematic change in the oxygen fugacity as function of *T*, *P*, and *nbo/t* can be excluded. The effective oxygen fugacity that had prevailed during the experiment was calculated after the experiment relative to the Fe-FeO equilibrium (IW) from the activities of Fe and FeO in the metal sulfide and silicate phases according to the following equation:

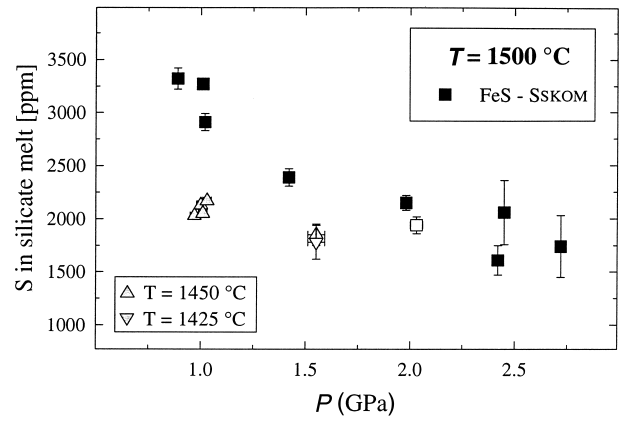

FIGURE 2. Sulfur concentration in the silicate melt as a function of pressure at constant temperature. Black squares represent experiments with SSKOM-silicate at 1500 °C. The open square illustrates the reversal experiment (see text for more detail). Gray symbols illustrate experiments at 1450 °C (upward triangles) and 1425 °C (downward triangle at 1.5 GPa) and are marked ("†") in Table 2.

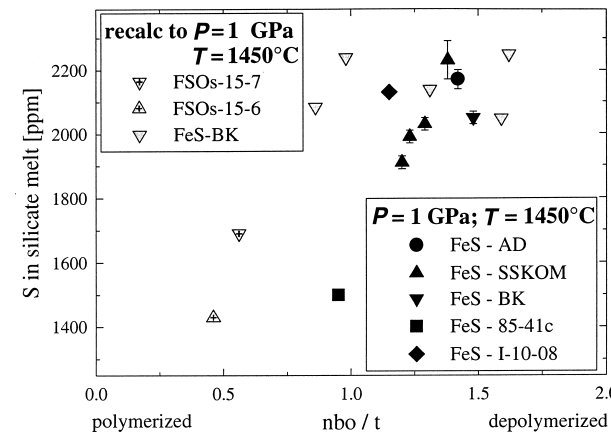

FIGURE 3. Sulfur concentration in the silicate melt as a function of the composition of the silicate melt at constant temperature (1450 °C) and pressure (1 GPa). The compositional variations in FeO-containing silicates are expressed as *nbo/t* values, i.e., the ratio of non-bridging oxygen atoms to tetrahedrally coordinated cations. The gray triangles are data of this study and the gray cross-haired triangles are data from Holzheid et al. (2000), both recalculated to 1450 °C and 1 GPa. The combined *T-P* dependence (see Table 7a) was used for recalculation. The S solubility in depolymerized silicate liquids is higher than in more-polymerized silicate liquids, suggesting that S reacts preferentially with non-bridging O atoms in the silicate melt.

$$\log f_{O_2}^{\text{experiment}} = \log f_{O_2}^{\text{IW}} + \Delta\text{IW} \quad (1)$$

$$\text{with } \Delta\text{IW} = 2 \cdot \log (a_{FeO}^{\text{silicate liquid}} / a_{Fe}^{\text{metal sulfide}}) = 2 \cdot \log (X_{FeO}^{\text{silicate liquid}} \cdot \gamma_{FeO}^{\text{silicate liquid}} / X_{Fe}^{\text{metal sulfide}} \cdot \gamma_{Fe}^{\text{metal sulfide}})$$

where $a_{FeO}^{\text{silicate liquid}}$ and $a_{Fe}^{\text{metal sulfide}}$ are the activities of FeO in the silicate liquid and Fe in the metal sulfide, $X_{FeO}^{\text{silicate liquid}}$ and $X_{Fe}^{\text{metal sulfide}}$ are the mole fractions of FeO in the silicate liquid and Fe in the metal sulfide, and $\gamma_{FeO}^{\text{silicate liquid}}$ and $\gamma_{Fe}^{\text{metal sulfide}}$ are the activity coefficients of FeO in the silicate liquid and Fe in the metal sulfide.

TABLE 4. Olivine and pyroxene compositions in wt%

Olivine		SiO_2	FeO	MnO	MgO	CaO	NiO	Total
FeS-SSKOM 11	*3*	40.6 (2)	9.85 (17)	0.159 (4)	49.1 (2)	0.226 (10)	0.017 (12)	100.1
FeS-SSKOM 7	*1*	40.8	9.01	0.192	49.4	0.259	0.031	99.8
FeS-SSKOM 5	*2*	41.1 (1)	8.07 (2)	0.198 (29)	50.3 (0)	0.260 (2)	0.070 (2)	100.1
FeS-SSKOM 6	*4*	41.1 (1)	8.19 (18)	0.165 (3)	50.4 (3)	0.241 (16)	0.055 (10)	100.2
FeS-SSKOM 1	*5*	39.1 (1)	15.8 (3)	0.271 (11)	44.3 (5)	0.305 (14)	0.086 (18)	100.1
FeS-SSKOM 2	*4*	39.0 (1)	15.3 (1)	0.264 (5)	45.2 (1)	0.348 (2)	0.037 (5)	100.4
FeS-SSKOM 14	*5*	40.5 (0)	11.7 (1)	0.156 (11)	47.4 (0)	0.187 (0)	0.023 (5)	100.1
FeS-SSKOM 25	*20*	40.8 (1)	9.86 (26)	0.155 (4)	48.8 (2)	0.144 (10)	0.036 (19)	99.9
FeS-SSKOM 26	*35*	41.9 (11)	9.15 (57)	0.167 (5)	48.0 (10)	0.217 (58)	0.038 (16)	99.7
FeS-SSKOM 15	*1*	40.4	11.1	0.169	48.1	0.196	0.034	100.1
FeS-SSKOM 16	*6*	40.4 (1)	11.9 (1)	0.188 (3)	47.3 (2)	0.352 (17)	0.025 (17)	100.3
FeS-SSKOM 27R	*15*	43.3 (14)	9.22 (56)	0.182 (6)	44.7 (18)	0.699 (249)	0.030 (14)	99.1
FeS-BK 9	*4*	41.2 (1)	7.75 (1)	0.104 (3)	50.4 (1)	0.548 (8)	0.064 (17)	100.2
FeS-BK 8	*15*	41.0 (0)	6.90 (3)	0.102 (2)	50.9 (1)	0.448 (17)	0.062 (11)	99.5
FeS-BK 4	*9*	40.7 (1)	7.13 (6)	0.095 (2)	52.2 (2)	0.447 (4)	0.043 (6)	100.7
FeS-BK 13	*15*	40.7 (1)	7.99 (39)	0.095 (6)	49.8 (3)	0.343 (26)	0.014 (10)	99.1
FeS-AD 1	*6*	41.5 (1)	5.98 (18)	0.103 (6)	52.0 (2)	0.555 (8)	0.037 (7)	100.3
FeS-85-41c-1	*1*	41.6	10.3	0.130	46.8	0.923	0.147	101.5
FeS-I-10-08-1	*4*	40.5 (2)	8.51 (2)	0.101 (7)	49.9 (3)	0.147 (8)	0.055 (27)	99.2
FSOs-15-6	*6*	40.6 (1)	10.4 (2)	0.120 (5)	49.0 (2)	0.132 (9)	0.290 (29)	100.6
FSOs-15-7	*7*	40.5 (1)	11.6 (1)	0.150 (9)	48.8 (1)	0.193 (16)	0.087 (28)	101.3

Pyroxene		SiO_2	Al_2O	FeO	MnO	MgO	CaO	Na_2O	Total
FeS-SSKOM 7	*6*	57.6 (1)	1.44 (1)	6.03 (2)	0.194 (5)	34.0 (1)	1.92 (1)	<d.l.	101.5
FeS-SSKOM 5	*6*	57.4 (1)	1.98 (9)	4.90 (2)	0.173 (5)	34.9 (1)	1.63 (3)	<d.l.	101.3
FeS-SSKOM 6	*3*	58.6 (1)	1.43 (5)	4.70 (17)	0.159 (5)	36.1 (2)	1.30 (2)	<d.l.	102.5
FeS-SSKOM 1	*11*	53.2 (2)	6.50 (30)	10.6 (1)	0.274 (4)	28.2 (2)	2.54 (4)	<d.l.	101.7
FeS-SSKOM 2	*10*	53.8 (1)	5.47 (12)	10.1 (1)	0.278 (8)	29.1 (2)	2.55 (5)	0.020 (3)	101.8
FSOs-15-6	*4*	53.6 (4)	8.55 (53)	7.48 (13)	0.108 (14)	28.4 (4)	2.21 (18)	0.457 (43)	100.8
FSOs-15-7	*16*	52.1 (2)	9.29 (28)	5.8 (12)	0.135 (6)	20.9 (3)	12.2 (4)	0.698 (20)	101.1
FSOs-15-7	*7*	54.0 (5)	7.07 (49)	7.26 (16)	0.124 (5)	30.4 (3)	2.10 (8)	0.156 (9)	101.1

Notes: Numbers in italic font are numbers of individual analyzes. Numbers in parentheses are 1 σ standard deviations of the mean. The entry should be read 40.6 ± 0.2 wt%. Experiments FeS-BK 1 and FeS-BK 10 are not included as the metal sulfide phase coexisted with subliquidus silicate starting material. <d.l. = below detection limit. Sulfur-content in olivine and pyroxene was below detection limit.

TABLE 5. Sulfide melt compositions in wt%

		Fe	Ni	Co	S	Total
FeS-SSKOM 13	*10*	62.2 (2)	0.60 (17)	0.16 (1)	35.7 (2)	98.6
FeS-SSKOM 12	*10*	62.7 (2)	0.43 (5)	0.16 (1)	35.2 (3)	98.5
FeS-SSKOM 11	*10*	63.3 (3)	0.64 (10)	0.18 (2)	34.6 (4)	98.7
FeS-SSKOM 7	*10*	61.2 (3)	0.75 (34)	0.18 (1)	36.7 (3)	98.8
FeS-SSKOM 5	*10*	60.9 (2)	0.75 (17)	0.17 (2)	36.8 (3)	98.6
FeS-SSKOM 6	*10*	61.1 (3)	1.68 (47)	0.20 (1)	35.7 (3)	98.7
FeS-SSKOM 1	*13*	69.1 (10)	0.47 (7)	0.25 (3)	28.8 (12)	98.6
FeS-SSKOM 2	*14*	67.3 (9)	0.49 (12)	0.21 (3)	30.7 (11)	98.7
FeS-SSKOM 14	*15*	58.8 (4)	6.16 (95)	0.35 (3)	34.0 (7)	99.3
FeS-SSKOM 25	7	62.0 (3)	0.67 (10)	0.07 (2)	36.3 (8)	99.0
FeS-SSKOM 26	5	60.1 (2)	0.91 (2)	0.10 (1)	39.4 (3)	100.6
FeS-SSKOM 15	*16*	64.4 (5)	1.15 (27)	0.22 (3)	32.7 (7)	98.5
FeS-SSKOM 16	*10*	62.0 (2)	0.36 (2)	0.13 (1)	35.8 (2)	98.3
FeS-SSKOM27R	*10*	59.5 (4)	1.08 (21)	0.07 (1)	38.6 (4)	99.3
FeS-SSKOM 23	10	62.3 (1)	0.22 (1)	0.15 (1)	36.7 (3)	99.4
FeS-SSKOM 17	7	61.9 (2)	0.76 (57)	0.17 (3)	35.3 (7)	98.1
FeS-SSKOM 24	9	61.5 (1)	0.27 (1)	0.16 (1)	37.5 (2)	99.4
FeS-BK 11	*8*	60.7 (6)	1.35 (59)	0.21 (1)	36.8 (1)	99.1
FeS-BK 12	*8*	59.6 (5)	2.00 (44)	0.22 (1)	36.3 (1)	98.1
FeS-BK 9	*7*	57.3 (7)	5.53 (106)	0.28 (1)	34.5 (4)	97.6
FeS-BK 8	*10*	54.7 (14)	8.75 (181)	0.29 (2)	34.0 (5)	97.7
FeS-BK 4	*5*	61.3 (2)	0.70 (3)	0.18 (1)	35.8 (2)	98.0
FeS-BK 13	*4*	58.5 (5)	3.67 (11)	0.12 (1)	36.9 (11)	99.2
FeS-AD 1	*10*	59.7 (5)	1.26 (56)	0.20 (1)	36.5 (1)	97.7
FeS-85-41c-1	*5*	60.8 (1)	0.24 (3)	0.17 (1)	36.2 (2)	97.4
FeS-I-10-08-1	*10*	60.4 (4)	2.27 (32)	0.21 (1)	35.4 (2)	98.3
FSOs-15-6	*5*	73.2 (9)	0.54 (13)	n.d.	25.0 (9)	98.7
FSOs-15-7	*5*	70.7 (3)	0.93 (12)	n.d.	26.8 (1)	98.4

Notes: Numbers in italic font are numbers of individual analyzes; Numbers in parentheses are 1 σ standard deviations of the mean. The entry should be read 62.2 ± 0.2 wt%. The analytical totals lower than 100 might be attributed to the presence of small amounts of oxygen in the metal phases. Experiments FeS-BK 1 and FeS-BK 10 are not included as the metal sulfide phase coexisted with subliquidus silicate starting material. n.d. = not determined.

We adopted the activity model of Li and Agee (1996), who assumed that the activity coefficients of FeO in the silicate liquid and Fe in the coexisting metal sulfide are close to unity. The calculated oxygen fugacities relative to the IW buffer are listed as ΔIW in Table 2. No systematic change of ΔIW as function of T, P, and nbo/t can be observed. The variation in S concentrations in silicate liquids, as graphically illustrated in Figures 1–3, therefore reflects largely the influence of T, P, and nbo/t on the S solubility in the silicate liquids at an oxygen fugacity approximately 1 to 2 log units below the IW buffer.

DISCUSSION

Comparison with literature data

Experimental studies on SSL in silicate liquids at elevated temperatures and pressures are summarized in Table 6.

In all hydrous experiments (Luhr 1990; Carroll and Rutherford 1987) and anhydrous, FeO-free experiments (Mysen and Popp 1980), oxygen fugacities were superimposed on the experimental charges by solid-buffer assemblages. Crystalline anhydrite ($CaSO_4$) coexisted with solid and liquid silicate phases in experiments at oxidized conditions (Fe_2O_3-Fe_3O_4, MnO-Mn_3O_4 buffers), whereas molten FeS was present in the reducing experiments (Ni-NiO , quartz-fayalite-magnetite buffers).

In anhydrous, FeO-containing experiments (Wendlandt 1982; Markus and Baker 1989; Jana and Walker 1997; Mavrogenes and O'Neill 1999; this study) Fe sulfide melt coexisted with solid and liquid silicate phases. These experiments

TABLE 6. Experimental studies on SSL in silicate liquids at elevated temperatures and pressures

Reference	Starting silicate	FeO-content of starting silicate (wt%)	T (°C)	P (GPa)	Observed solubility effect
		Temperature dependence			
Hydrous, FeO-containing experiments*					
Luhr (1990)	andesite, basalt	5.5–7.6	800–1000	0.2	S ↑ w/ T↑
Carroll and Rutherford (1987)	trachyandesite	≤ 8	850–1027	0.2	S ↑ w/ T↑
Anhydrous, FeO-containing experiments†					
Wendlandt (1982)	andesite, basalt	5.4–17	1300–1460	2	S ↑ w/ T↑
Markus and Baker (1989)	andesite	5.5	1200–1400	1	S ↑ w/ T↑
Mavrogenes and O'Neill (1999)	basalt	10.5	1400–1800	0.5	S ↑ w/ T↑
			1400–1500	1.5	S ↑ w/ T↑
Jana and Walker (1997)	komatiite	16–33	1800–2200	5	no T-effect
this study	MgO-rich basalt	5.2–12	1350–1600	1	S ↑ w/ T↑
Anhydrous, FeO-free experiments‡					
Mysen and Popp (1980)	$NaAlSi_3O_8$		1450–1650	3	S ↑ w/ T↑
		Pressure dependence			
Hydrous, FeO-containing experiments					
Carroll and Rutherford (1985)	dacite	≤8	1025	0.1–0.2	no P-effect
Carroll and Rutherford (1985)	dacite	10–30	1025	0.1–0.2	S ↑ w/ P↑
Anhydrous, FeO-containing experiments					
Wendlandt (1982)	andesite, basalt	5.4–17	1420	1.3–3	S ↓ w/ P↑
Mavrogenes and O'Neill (1999)	basalt	10.5	1400	0.5–3.5	S ↓ w/ P↑
			1500	0.5–2.5	S ↓ w/ P↑
			1800	0.5–9	S ↓ w/ P↑
	picrite	10.1	1500	0.5–1.5	S ↑ w/ P↑
			1800	1–4	S ↓ w/ P↑
This study	MgO-rich basalt	5.2–12	1450	1–1.5	S ↓ w/ P↑
			1500	0.9–2.7	S ↓ w/ P↑
Anhydrous, FeO-free experiments					
Mysen and Popp (1980)	$NaAlSi_3O_8$		1650	1.5–3	S ↑ w/ P↑
	$CaMgSi_2O_6$		1650	1.5–3	S ↑ w/ P↑

Note: S ↑ or ↓ w/ T or P↑: SSL increase or decrease with increasing T or P.
* Experimental device: TZM (titanium-zirconium-molybdenum) and/or internally heated pressure vessels.
† Experimental device: piston cylinder.
‡ Experimental device: piston cylinder.

were not buffered with a solid oxygen buffer assemblage. However, the intrinsic oxygen fugacities of the assemblages were influenced by the different capsule material used in the studies. Graphite was used by Wendlandt (1982), Markus and Baker (1989), and Jana and Walker (1997), whereas olivine was used as capsule material in this study. Pure Fe metal and FeIr alloys ($Fe_{40}Ir_{60}$, $Fe_{20}Ir_{80}$) were used by Mavrogenes and O'Neill (1999) to impose three distinct oxygen fugacities relative to the IW buffer on the experimental charge (2 log units of f_{O_2} below IW, 0.5 and 2 log units of f_{O_2} above IW).

Despite the differences in the experimental parameters (e.g., hydrous vs. anhydrous, oxygen fugacities, FeO-content in the silicate liquid), an increase in the SSL in the liquid silicate phases with increasing temperature was observed in all experimental studies, with the exception of the study of Jana and Walker (1997), who report no significant effect of temperature on the SSL in the liquid silicate. The S concentrations in the silicate liquids reported by Jana and Walker (1997) vary by factors of up to 1.4 in experiments with identical experiment conditions (T, P). This variation might reflect the lack of reproducibility of these experiments.

Sulfur solubilities in FeO-containing systems decrease with increasing pressure at constant temperatures (Wendlandt 1982; Mavrogenes and O'Neill 1999; this study). The pressure dependence observed in our study and also by Mavrogenes and O'Neill (1999) is more pronounced at lower pressure than at higher pressures. Mysen and Popp (1980) reported an increase in S solubility with increasing pressure in both FeO-free silicate liquids that they studied (diopside and albite). Diopside melt dissolves significantly more S than albite melt, suggesting that S reacts preferentially with non-bridging oxygen. This inference is in agreement with the observation of higher SSL in less-polymerized FeO-containing silicate liquids (Haughton et al. 1974). An increase in the S content in the silicate liquid with pressure, as found by Mysen and Popp (1980), is in agreement with the S solubility dependence on pressure in hydrous experiments with FeO-concentrations greater than 10 wt% in the silicate liquid (Table 6; Carroll and Rutherford 1985). Despite some controversial observations and interpretations (Kohn et al. 1992, 1994; Sykes and Kubicki 1993, 1994), water ruptures intertetrahedral linkages in silicate melt structures and depolymerizes the silicate melt. As the water solubility increases

with increasing total pressure in water-saturated melts at isothermal conditions (e.g., Dingwell 1986; Burnham 1994 and references therein), the silicate melt at the highest pressure in the study by Carroll and Rutherford (1985) is less polymerized than it is at lower pressures, allowing more S to be dissolved in the silicate liquid at higher than at lower pressures. This depolymerization mechanism influences the pressure dependence of S solubility in hydrous silicate melt. It is the influence of the increased H_2O solubility rather than the effect of the total pressure that leads to an increase in the S content. However, the S-solubility dependence on pressure observed by Mysen and Popp (1980) is the opposite of all other results in anhydrous assemblages (Wendlandt 1982; Mavrogenes and O'Neill 1999; this study). This difference might be related to the different capsule materials used in the studies and their influences on the stable S species in the coexisting solid and liquid silicate phases. Mysen and Popp (1980) used boron nitride, which imposes very reducing conditions on the experimental charge (T.L. Grove, unpublished data). The different f_{O_2}–f_{S_2} conditions and the absence of FeO in the silicate liquid studied by Mysen and Popp (1980) may have altered the stable S species in the melt, e.g., dissolution of S^{2-} vs. Fe-S-O-species in silicate melts. This speciation might cause the drastic differences in the absolute SSL and the different pressure observations described in the solubility studies.

Based on the thermodynamic equilibrium relation between FeO in the silicate liquid and FeS in the metallic sulfide, Mavrogenes and O'Neill (1999) derived the following equation (their Equation 10) to calculate the expected SSL in liquid silicate at certain *T*-*P*-conditions.

$$\ln S = A / T + B + C\,(P/T) + \ln a_{FeS}^{sulfide} \quad (2)$$

where the S-content in the silicate liquid is in ppm, temperature T in Kelvin, and pressure P in bar.

We fit our experimental SSKOM and BK data to Equation 2, assuming the activity of FeS in the metallic sulfide, $a_{FeS}^{sulfide}$, to be around 1 as our metallic sulfides are close to stoichiometric FeS (see also Mavrogenes and O'Neill 1999). The fit excluded the 3 time-series experiments and the subliquidus experiments. The results of the non-linear least-squares regression of the SSL in liquid silicate are listed in Table 7a. Fit parameters of the experimental results on the SSL in anhydrous, FeO-containing systems (Mavrogenes and O'Neill 1999; Wendlandt 1982) are also listed in Table 7a. The empirically derived parameter of all three studies agree within 1σ except for Grand Ronde Basalt (Wendlandt 1982) with a slightly higher B parameter and Mt. Hood Andesite (Wendlandt 1982). However, even these exceptions agree within 2σ. The reason for the gradual change in agreement between the Wendlandt-data and our study (or that of Mavrogenes and O'Neill 1999) might be attributed to the significant change of the SSL in polymerized silicate liquids (*nbo*/*t*-ratios <0.9; see Fig. 3), as at least the three silicate starting materials used by Wendlandt (1982) have *nbo*/*t*-ratios from 0.2 to 0.7 with $nbo/t_{\text{Goose Island Basalt}} > nbo/t_{\text{Grand Ronde Basalt}} >> nbo/t_{\text{Mt. Hood Andesite}}$. Unfortunately, the silicate liquid compositions of the experimental products are not reported by Wendlandt (1982).

We can assess the dependence of S-solubility on the silicate liquid composition by adding an *nbo*/*t* parameter. Equation 2 then becomes

$$\ln S = A / T + B + C\,(P/T) + D\ nbo/t + \ln a_{FeS}^{sulfide} \quad (3)$$

where the S-content in the silicate liquid is in ppm, temperature T in Kelvin, pressure P in bar, and $a_{FeS}^{sulfide} \sim 1$.

We fit our experimental data for SSKOM, BK, AD, 85–41c, I-10-08, and SB to Equation 3. The three time-series experiments and the subliquidus experiments are again excluded. As Mavrogenes and O'Neill (1999) reported the chemical compositions of their experimental products, we also fit their data to Equation 3. The results of both non-linear least-squares regressions of the S solubility limits in liquid silicate as function of T, P, and *nbo*/*t* are listed in Table 7b. The empirically de-

TABLE 7A. Parameters of the non-least squares regression of the experimentally determined SSL in silicate liquids at elevated temperatures and pressures

Reference	No.	Starting silicate	A	B	C	r^2
This study	20	SSKOM, BK	–8120 (1505)	12.64 (0.87)	–0.040 (0.009)	0.736
Mavrogenes and O'Neill (1999)	23	Basalt	–14056 (2093)	15.50 (1.26)	–0.062 (0.011)	0.731
Wendlandt (1982)	6	G.R.Basalt	–9692 (1143)	13.67 (0.68)	–0.053 (0.007)	0.979
Wendlandt (1982)	6	G.I.Basalt	–8487 (388)	13.13 (0.23)	–0.035 (0.002)	0.997
Wendlandt (1982)	6	M.H.Andesite	–18014 (558)	18.63 (0.33)	–0.099 (0.003)	0.999

Notes: Standard deviations are in parentheses; no. = number of observations that are fitted. ln S [ppm] = A / *T*[K] + B + C (*P*[bar] / *T*[K]).

TABLE 7B. Parameters of the non-least squares regression of the experimentally determined SSL in silicate liquids at elevated temperatures and pressures

Reference	No.	A	B	C	D	r^2
This study	25	–7714 (2582)	11.90 (1.65)	–0.038 (0.012)	0.368 (0.169)	0.731
Mavrogenes and O'Neill (1999)	28	–12012 (2122)	13.87 (1.38)	–0.061 (0.011)	0.712 (0.327)	0.749
this study and Mavrogenes and O'Neill (1999)	53	–10129 (1601)	12.84 (1.02)	–0.060 (0.009)	0.793 (0.159)	0.744

Notes: Standard deviations are in parentheses; no. = number of observations that are fitted; starting silicates = SSKOM, BK, AD, 85–41c, I–10–08, SB (this study, see Table 1); basalt, picrite (Mavrogenes and O'Neill 1999). ln S [ppm] = A / *T*[K] + B + C (*P*[bar] / *T*[K]) + D *nbo/t*.

rived parameter of both studies agree within ~1σ. In addition, we combined both studies and fit the larger dataset to Equation 3. The parameter of the single non-linear least-squares regression is also listed in Table 7b.

Implications of the sulfur solubility limits for sulfide saturation in primitive mantle-derived melts

The variation of the sulfur solubility limit in an ascending magma with an *nbo*/*t*-ratio >0.9 is shown in Figure 4. The *T*-*P* change during the ascent based on an adiabatic decompression melting path of 30 °C/GPa from McKenzie and Bickle (1988) is plotted as a black curve. The inferred depth for magma segregation of MORB picrite (2 GPa, 1430 °C) from Green et al. (1979) was used as the starting *T*-*P* conditions at the beginning of the ascent. The expected S-solubility during adiabatic decompression melting is calculated using the regression parameters given in Table 7a. The negative pressure dependence of sulfur solubility is more influential than the positive temperature dependence along the adiabatic uplift path. Therefore, adiabatic decompression melting will lead to S undersaturation, if the initial melt is S saturated. This confirms the findings by Mavrogenes and O'Neill (1999). A primitive magma that is S saturated in its source region will become S undersaturated as it ascends to shallower depth. In order to precipitate magmatic sulfides, the magma must first cool and undergo fractional crystallization to reach S saturation. Thus, resupply of primitive magma into an open-system magma chamber is not likely to trigger S saturation, in fact the opposite will happen. This finding has implications for models of ore formation that rely on injections of primitive magma into evolving magma chambers. Furthermore, the S capacity of polymerized melts is lower than that of depolymerized melts (e.g., primitive magmas). Mixing of polymerized and depolymerized magmas could trigger S saturation but it would be the result of the influence of the polymerized melt in lowering the S capacity of the magma mixture. These constraints are important for models of S saturation in magmatic sulfide deposits that call upon magma mixing to trigger the S saturation of the magma (e.g., Irvine et al. 1983).

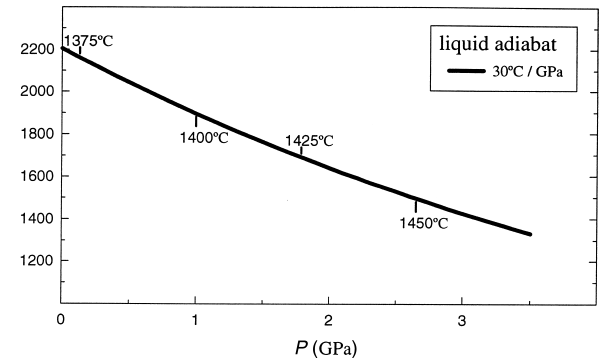

FIGURE 4. Calculated S solubility limits in an ascending magma as a function of temperature and pressure. The *T*-*P* change during the ascent is based on a liquid adiabatic gradient of 30 °C/GPa. The S solubility limit in a silicate liquid decreases with increasing temperature and pressure. The ascending magma will therefore arrive at the surface S undersaturated although the silicate was S saturated in its source region. This is even the case for the magma with the higher S concentration in the magma's source region and a faster uplift rate.

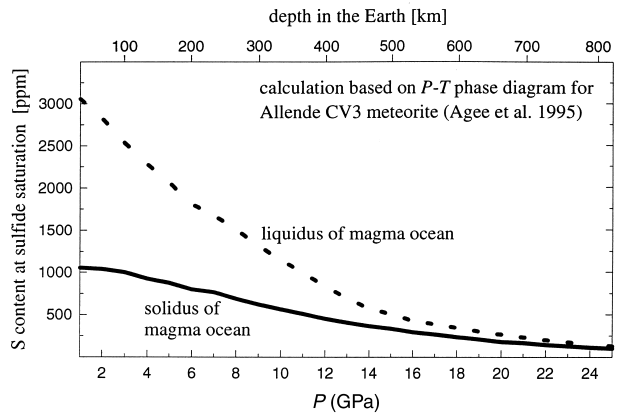

FIGURE 5. Calculated S solubility limit in a terrestrial magma ocean. The range of the S content in a magma ocean extending to a depth of 750 km (P = 23 GPa) will be close to the S content in the present-day Earth's bulk mantle if the light element in the core is exclusively S.

Implications of the sulfur solubility limits for metal-silicate separation scenarios

If a terrestrial magma ocean was saturated with respect to a metal sulfide phase, the average S content in that magma ocean can be also inferred from the results of the experimental studies. Li and Agee (1996) experimentally determined liquid alloy (FeNiCoS-bearing alloy)-liquid silicate (Allende CV3 meteorite) partition coefficients at pressures of 2 to 20 GPa. Based on their findings, Li and Agee (1996) concluded that the absolute and relative abundances of Ni and Co in the present-day terrestrial mantle are consistent with an alloy-silicate equilibrium at high pressures. They therefore implied the presence of a magma ocean with a minimum depth of 750 km (~23 GPa) at the time of terrestrial core formation. We will use the combined *T*-*P* dependence of the S solubility measured in this study (Table 7a) to extrapolate the S solubility to the conditions of a magma ocean with a depth of 750 km. The expected S concentration in a terrestrial magma ocean is graphically illustrated as function of temperature and pressure in Figure 5. We used the temperature vs. pressure phase diagram for the Allende CV3 carbonaceous chondrite (Agee et al. 1995) to calculate the S solubility at the liquidus and solidus conditions of the magma ocean. Because carbonaceous chondrites are assumed to be one of the major building blocks of the Earth, the *T*-*P* relationship of the Allende CV3 meteorite is appropriate for an analogue of the *T*-*P* relations of a terrestrial magma ocean. Because the pressure dependence of the S solubility in silicate liquids is more pronounced at lower pressure than at higher pressure, the decrease of the expected S concentration in the magma ocean as function of pressure, i.e., depth of the magma ocean, is more pronounced at the shallower part of the magma ocean than at the base of the magma ocean. To account for the difference in the slope of the S solubility as function of pressure, the magma ocean has been divided into two parts. The integrated S con-

centration in the magma ocean was calculated based on the averaged S contents of both parts. The range of averaged S contents of the part of the magma ocean that extends from the surface to a pressure of 14 GPa is ~800 to ~1800 ppm. The 800 ppm value reflects the S content at the *T-P* conditions slightly higher than the solidus conditions of the magma ocean. The S content at the liquidus *T-P* conditions of the magma ocean is 1800 ppm. The mass proportion of the first part is ~58% relative to the entire magma ocean. The range of averaged S contents in the part that extends from 14 GPa to 23 GPa (42% of the entire magma ocean) is ~300 ppm at *T-P* conditions slightly higher than the solidus conditions of the magma ocean and ~425 ppm at the liquidus *T-P* conditions of the magma ocean. The averaged minimum S concentration of the entire magma ocean would be ~590 ppm and the averaged maximum S concentration would be ~1225 ppm. The calculated S concentration assumes equilibrium of the magma ocean with metallic liquids like those in our experiments under oxygen fugacity conditions similar to those of our experiments.

If the lower density of the Earth's metallic core is exclusively due to the presence of S as the light element, the metal sulfide that formed the core would contain 9–12 wt% S (Ahrens 1979). The S concentration of a silicate magma ocean in equilibrium with a metal sulfide melt containing S abundances in this range would be ~175 to ~370 ppm. Note that these values are within the range of estimates from our sulfide-saturation model for a magma ocean that was in equilibrium with a metal sulfide melt. The nature of the light element(s) that is (are) sequestered in the Earth's core is a matter of debate. The lower density of the metallic core may be due to the presence of several light elements, e.g., C, O, N, Si, and H, in addition to some S. Dreibus and Palme (1996) estimated from cosmochemical constraints a maximum S content of the Earth's core of 1.7 wt%. A magma ocean that was in equilibrium with a metallic liquid that contains only 1.7 wt% sulfur would have a S concentration between ~30 and ~60 ppm.

The upper and lower limit of the expected S content in a terrestrial magma ocean that is in equilibrium with a metallic liquid that contains 9–12 wt% sulfur agrees well with the estimates of the S content in the present-day Earth's bulk mantle. Calculation of the expected S content in a magma ocean that is in equilibrium with a metallic liquid that contains only 1.7 wt% sulfur is lower than the mantle estimates of O'Neill (1991) and McDonough and Sun (1995), but agrees with the estimated mantle S content of Dreibus and Palme (1996).

Estimates of the S content in the present-day Earth's bulk mantle range from ~124 ± 90 ppm (Dreibus and Palme 1996) to ~250 ± 50 ppm (McDonough and Sun 1995). O'Neill (1991) estimated an average S content in the upper mantle of ~200 ppm. An average S content in the upper mantle of ~200 ppm is covered by all three estimates for the S content in the present-day Earth's bulk mantle. The S content in a metallic liquid that is in equilibrium with a hot magma ocean that contains ~200 ppm S ranges from 5.5 to 12 wt% S, assuming an equilibrium distribution of sulfur between the magma ocean and the metallic liquid as outlined in the preceding model. Our experimental results may provide an estimate of the S content in the metallic phase that formed the Earth's core.

ACKNOWLEDGMENTS

This research was performed while the first author held a research scholarship supported by the German Science Foundation (DFG). Support for this research was also provided by NASA Grant NAG-5-4768 to TLG. Comments by the Associate Editor J.H. Jones, referees K. Righter and G.A. Gaetani, and an anonymous referee on an earlier version of the manuscript are appreciated.

REFERENCES CITED

Abraham, K.P. and Richardson, F.D. (1960) Sulfide capacities of silicate melts. Part II. Journal of The Iron and Steel Institute, 196, 313–317.

Abraham, K.P., Davies, M.W., and Richardson, F.D. (1960) Sulfide capacities of silicate melts. Part I. Journal of The Iron and Steel Institute, 196, 309–312.

Agee, C.B., Li, J., Shannon, M.C., and Circone, S. (1995) Pressure-temperature phase diagram for the Allende meteorite. Journal of Geophysical Research, 100, 17725–17740.

Ahrens, T.J. (1979) Equation of state of iron sulfide and constraints on the sulfur content of the Earth. Journal of Geophysical Research, 84, 985–998.

Armstrong, J.T. (1995) CITZAF-A package for correction programs for the quantitative electron microbeam x-ray analysis of thick polished materials, thin-films and particles. Microbeam Analyzes, 4, 177–200.

Baker, M.B., Grove, T.L., and Price, R. (1994) Primitive basalts and andesites from the Mt.Shasta region, N.California: products of varying melt fraction and water content. Contributions to Mineralogy and Petrology, 118, 111–129.

Boyd, F.R. and England, J.L. (1960) Apparatus for phase-equilibrium measurements at pressures up to 50 kilobars and temperatures up to 1750 °C. Journal of Geophysical Research, 65, 741–748.

Burnham, C.W. (1994) Development of the Burnham model for prediction of H_2O solubility in magmas. In M.R. Carroll and J.R. Holloway, Eds., Volatiles in magmas, pp.123–129. Reviews in Mineralogy, 30. Mineralogical Society of America, Washington, D.C.

Carmichael, I.S.E. (1967) The mineralogy and petrology of the volcanic rocks from the Leucite Hills, Wyoming. Contributions to Mineralogy and Petrology, 15, 24–66.

Carroll, M.R. and Rutherford, M.J. (1985) Sulfide and sulfate saturation in hydrous silicate melts. Proceedings of the fifteenth Lunar and Planetary Science Conference, part 2. Journal of Geophysical Research-Supplement, 90, C601-C612.

———(1987) The stability of igneous anhydrite: experimental results and implications for sulfur behavior in the 1982 El Chichon trachyandesite and other evolved magmas. Journal of Petrology, 28, 781–801.

Dingwell, D.B. (1986) Volatile solubilities in silicate melts. In C.M. Scarfe, Ed., Silicate melts-their properties and structure applied to problems in geochemistry, petrology, economic geology and planetary geology, pp. 93–129. MAC Short Course Handbook, 12. Mineralogical Association of Canada, Toronto.

Dreibus, G. and Palme, H. (1996) Cosmochemical constraints on the sulfur content in the earth's core. Geochimica et Cosmochimica Acta, 60, 1125–1130.

Fincham, C.J.B. and Richardson, F.D. (1954) The behavior of sulfur in silicate and aluminate melts. Proceedings of the Royal Society of London, 223A, 40–62.

Green, D.H., Hibberson, W.O., and Jaques, A.L. (1979) Petrogenesis of mid-ocean ridge basalts. In M.W. McElhinny, Ed., The Earth: Its Origin, Structure and Evolution, pp. 265–290, Academic Press, London.

Haughton, D.R., Roeder, P.L., and Skinner, B.J. (1974) Solubility of sulfur in mafic magmas. Economic Geology, 69, 451–467.

Holzheid, A. and Palme, H. (1996) The influence of FeO on the solubilities of Co and Ni in silicate melts. Geochimica et Cosmochimica Acta, 60, 1181–1193.

Holzheid, A., Schmitz, M.D., and Grove, T.L. (2000) Textural equilibria of iron sulfide liquids in partly molten silicate aggregates and their relevance to core formation scenarios. Journal of Geophysical Research, 105 (B6), 13555–13567.

Irvine, T.N., Keith, D.W., and Todd, S.G. (1983) The J-M platinum-palladium reef of the Stillwater complex, Montana: II. origin by double-diffusive convective magma mixing and implications for the Bushveld complex. Economic Geology, 78, 1287–1334.

Jana, D. and Walker, D. (1997) The influence of sulfur on partitioning of siderophile elements. Geochimica et Cosmochimica Acta, 61, 5255–5277.

Kinzler, R.J. and Grove, T.L. (1985) Crystallization and differentiation of archean komatiite lavas from northeast Ontario: phase equilibrium and kinetic studies. American Mineralogist, 70, 40–51.

Kohn, S.C., Dupree, R., and Mortuza, M.G. (1992) The interaction between water and aluminosilicate magmas. Chemical Geology, 96, 399–409.

Kohn, S.C., Smith, M.E., and Dupree, R. (1994) Comment on "A model for H_2O solubility mechanisms in albite melts from infrared spectroscopy and molecular orbital calculations" by D. Sykes and J.D. Kubicki. Geochimica et Cosmochimica Acta, 58, 1377–1380.

Li, J. and Agee, C. B. (1996) Geochemistry of mantle-core formation at high pressure, Nature, 381, 686–689.

Luhr, J.F. (1990) Experimental phase relations of water- and sulfur-saturated arc magmas and the 1982 eruptions of El Chichón volcano. Journal of Petrology, 31, 1071–1114.

Markus, R.S. and Baker, D.R. (1989) Sulfur solubility in anhydrous andesitic melts.

EOS Transactions-American Geophysical Union, 70, 1402.
Mavrogenes, J.A. and O'Neill, H.St.C. (1999) The relative effects of pressure, temperature and oxygen fugacity on the solubility of sulfide in mafic magmas. Geochimica et Cosmochimica Acta, 63, 1173–1180.
McDonough, W.F. and Sun, S.-S. (1995) The composition of the earth. Chemical Geology, 120, 223–253.
McKenzie, D. and Bickle, M.J. (1988) The volume and composition of melt generated by extension of the lithosphere. Journal of Petrology, 29, 625–679.
Mysen, B.O. (1988) Structure and Properties of silicate melts. Elsevier, Amsterdam.
Mysen, B.O. and Popp, R.P. (1980) Solubility of sulfur in $CaMgSi_2O_6$ and $NaAlSi_3O_8$ melts at high pressure and temperature with controlled f_{O_2} and f_{S_2}. American Journal of Science, 280, 78–92.
O'Neill, H.St.C. (1991) The origin of the moon and the early history of the earth-a chemical model. part 2: the earth. Geochimica et Cosmochimica Acta, 55, 1159–1172.
Poulson, S.R. and Ohmoto, H. (1990) An evaluation of the solubility of sulfide sulfur in silicate melts from experimental data and natural samples. Chemical Geology, 85, 57–75.
Sykes, D. and Kubicki, J.D. (1993) A model for H_2O solubility mechanisms in albite melts from infrared spectroscopy and molecular orbital calculations. Geochimica et Cosmochimica Acta, 57, 1039–1052.
———(1994) Reply to the comment by S.C. Kohn, M.E. Smith, and R. Dupree on "A model for H_2O solubility mechanisms in albite melts from infrared spectroscopy and molecular orbital calculations." Geochimica et Cosmochimica Acta, 58, 1381–1384.
Wallace, P. and Carmichael, I.S.E. (1992) Sulfur in basaltic magmas. Geochimica et Cosmochimica Acta, 56, 1863–1874.
Wendlandt, R.F. (1982) Sulfide saturation of basalt and andesite melts at high pressures and temperatures. American Mineralogist, 67, 877–885.

MANUSCRIPT RECEIVED AUGUST 11, 2000
MANUSCRIPT ACCEPTED OCTOBER 18, 2001
MANUSCRIPT HANDLED BY JOHN H. JONES